Molecular Cancer

RESEARCH Open Access

Overcoming multi-drug resistance in SCLC: a synergistic approach with venetoclax and hydroxychloroquine targeting the lncRNA LYPLAL1-DT/BCL2/BECN1 pathway

Shuxin Li[1,2,3†], Jianyi Lv[1,2,3†], Zhihui Li[1,2,3†], Qiuyu Zhang[1,2,3†], Jing Lu[1,2,3], Xueyun Huo[1,2,3], Meng Guo[1,2,3], Xin Liu[1,2,3], Changlong Li[1,2,3], Jinghui Wang[4], Hanping Shi[2,5], Li Deng[2,5], Zhenwen Chen[1,2,3] and Xiaoyan Du[1,2,3*]

Abstract

Background Small cell lung cancer (SCLC) stands as one of the most lethal malignancies, characterized by a grim diagnosis and prognosis. The emergence of multi-drug resistance poses a significant hurdle to effective therapy. Although previous studies have implicated the long noncoding RNA LYPLAL1-DT in the tumorigenesis of SCLC, the precise role of the highly expressed LYPLAL1-DT in SCLC chemoresistance and the underlying mechanism remain inadequately understood.

Methods cDDP-, VP-16- and PTX-resistant SCLC cells lines were established. The viabilities of SCLC cells were assessed by CCK-8 assay in vitro and xenograft tumor formation assay in vivo. Apoptosis was evaluated by FACS, Western blot and JC-1 fluorescence staining, while autophagy was explored via autophagic flux detection under confocal microscopy and autophagic vacuole investigation under transmission electron microscopy (TEM). The functional role and mechanism of LYPLAL1-DT were further investigated by gain- and loss-of-function assays in vitro. Furthermore, the therapeutic efficacy of the combination of venetoclax and HCQ with cDDP, VP-16 or PTX was evaluated by cell line, cell-derived xenograft (CDX) and patient-derived xenograft (PDX) mice model.

Results Our findings revealed that LYPLAL1-DT is upregulated in chemoresistant SCLC cell lines. Gain- and loss-of-function assays demonstrated that LYPLAL1-DT impairs sensitivity to cDDP, VP-16, or PTX both in vitro and in vivo. Overexpression of LYPLAL1-DT significantly enhanced autophagy and inhibited apoptosis in SCLC cells. Further analyses, including RIP and RNA pull-down assays, revealed that LYPLAL1-DT promotes the expression of BCL2 by sponging miR-204-5p and is implicated in the assembly of the autophagy-specific complex (BECN1/PtdIns3K complex). Combining venetoclax and HCQ with cDDP, VP-16, or PTX effectively mitigated chemoresistance in SCLC cells and suppressed tumor growth in CDX and PDX models without inducing obvious toxic effects.

†Shuxin Li, Jianyi Lv, Zhihui Li and Qiuyu Zhang contributed equally to this work.

*Correspondence:
Xiaoyan Du
duduyan@ccmu.edu.cn

Full list of author information is available at the end of the article

Conclusions Our findings demonstrate that upregulation of LYPLAL1-DT sequesters apoptosis through the LYPLAL1-DT/miR-204-5p/BCL2 axis and promotes autophagy by facilitating the assembly of the BECN1/PtdIns3K complex, thereby mediating multi-drug resistance of SCLC. The triple combination of venetoclax, HCQ, in conjunction with cDDP, VP-16 or PTX overcomes refractory SCLC, shedding light on a potential therapeutic target for combating SCLC chemoresistance.

Keywords LYPLAL1-DT, BCL2, BECN1, Apoptosis, Autophagy, Multi-drug resistance, Small cell lung cancer

Introduction

Small cell lung cancer (SCLC), which accounts for 13%–15% of all lung cancers, stands as the sixth most common cause of cancer-related mortality worldwide [1–3]. SCLC is characterized by a rapid doubling time, high proliferation capacity and early extensive metastasis [4]. Despite advancements in diagnosis and treatment modalities, the prognosis for SCLC remains grim, primarily due to the rapid emergence of resistance to various therapeutic agents.

Etoposide-platinum remains the most common initial treatment regimen for SCLC. While most patients initially respond to chemotherapy, only approximately 10% remain disease-free after 2 years, remains would experience relapse after first-line treatment [5]. Chemoresistance even occurs for the second line treatments such as paclitaxel. Thus, multi-drug resistance (MDR) has emerged as a paramount concern in the management of SCLC.

The development of MDR in SCLC is a multifaceted process, involving a complex interplay of genetic, epigenetic, and microenvironmental factors. Dysregulated apoptosis and autophagy pathways are two key molecular contributors to this process [6]. Decreased apoptotic signaling, particularly the activating anti-apoptotic system, allows cancer cells to evade chemotherapy, leading to uncontrolled cell proliferation, tumor survival, drug resistance and cancer recurrence [7]. Aberrantly increased levels of B-cell lymphoma 2 (BCL2) is correlated with the development and poor prognosis of various cancers [8–10]. Targeting BCL2 inactivation has emerged as one of the most promising approaches combating various types of cancers [11, 12]. The small molecule BCL2 inhibitor ABT-199, known commercially as venetoclax, has shown considerable clinic efficacy in chronic leukemia, acute myeloid leukemia, and multiple myeloma [13–15]. Timothy L Lochmann et al. demonstrated that venetoclax induces regressions in high BCL2-expressing SCLC tumors in vivo, suggesting its potential application in a substantial fraction of SCLC cases. However, venetoclax-based regimens also confront dilemma of drug resistance [16–18]. Autophagy is a cellular survival mechanism that could be induced by various of stimuli or stress, such as food deprivation, hypoxia and chemotherapeutics [19, 20]. Numerous studies have shown that autophagy empowers tumor cells to overcome stresses and contributes to the chemoresistance [21, 22]. Inhibition of autophagy potentiates the chemosensitivity of breast cancer, prostate cancer and gastrointestinal stromal tumor cells [23–25]. Our previous study also illustrated that autophagy plays a protective role in the cisplatin-resistant SCLC cell line H446/cDDP and inhibition of autophagy enhances cisplatin-induced cell death [26]. The underlying molecular mechanism is an obscurity.

Long noncoding RNAs (lncRNAs) consist of more than 200 nucleotides and do not encode functional proteins. Accumulating evidence indicates that lncRNAs closely participate in cancer drug resistance by regulating miRNA, signaling pathways, cancer stem cells, pro- and anti-apoptosis, and autophagy [27–30]. Our previous studies revealed that lncRNA LYPLAL1-DT (Ensembl ID: ENSG00000228063) plays a protective role for endothelial cell under high-glucose and inflammatory condition [31] and is closely related to the malignant phenotype of SCLC [32]. This fact intrigues us to explore its effects on the chemoresistance of SCLC and the molecular mechanism behind.

In the current study, we show for the first time that LYPLAL1-DT promotes multi-drug resistance of SCLC by suppressing apoptosis and enhancing autophagy pathway. Combination of venetoclax and HCQ can significantly potentiate the sensitivity of SCLC cells to the primary chemotherapy regimens with no observed toxic effect. It offers a novel solution for SCLC and might eventually prolong the survival of patients.

Methods

Tissue specimens and serum samples

Serum samples of 8 chemotherapy-sensitive patients and 9 chemotherapy-resistance patients were collected from the Beijing Chest Hospital. Six paraffin-embedded tissue specimens from chemotherapy-sensitive patients and six from chemotherapy-resistance patients were also obtained from Beijing Chest Hospital. All samples were confirmed via pathologic examination. Informed consent was obtained from all patients prior to specimen collection, in accordance with institutional guidelines. All protocols were approved by the Institutional Review Board and informed consent was obtained from the patients or their guardians.

Cell lines, reagents, and antibodies

The lung cancer cell lines NCI-H446, NCI-H196 were obtained from the Chinese National Infrastructure of Cell Line Resource. Cells were maintained in RPMI1640 supplemented with 10% FBS (VisTech, New Zealand). All cell lines were cultured at 37 ℃ with 5% CO_2. The H446/cDDP, H446/VP-16, H446/PTX, H196/cDDP, H196/VP-16, H196/PTX chemo-resistant SCLC cell lines were established by our laboratory. H446 cells or H196 were treated with increased concentration of cisplatin, VP-16, or PTX. After 9–11 months of induction and screening, the final surviving cells showed resistance against cisplatin, VP-16 or PTX. Cisplatin and venetoclax were purchased from MedChemExpress (Cat#HY-17394, Cat#HY-15531). Hydroxychloroquine (HCQ) was purchased from MedChemExpress (Cat#HY-W031727) and Chongqing Kangle Pharmaceutical Co., Ltd (Cat#747-36-4). Etoposide (VP-16) and Paclitaxel (PTX) was purchased from meilunbio (Cat#MB1102-1 and Cat#MB1178-S). Commercially available antibodies are as follows: Anti-β-actin (HUABIO, Cat#R1207-1), anti-p62/SQSTM1 (Proteintech, Cat#18420-1-AP), anti-LC3B (HUABIO, ET1701-65), anti-casepase3 (Abcam, ab184787), anti-BCL2 (Abways, Cat#CY6717), anti-Beclin1/BECN1(Proteintech, Cat#11306-1-AP), anti-PIK3C3/VPS34 (Proteintech, Cat#12452-1-AP), anti-ATG14 (ABclonal, Cat#A7526), anti-Ago2 (CST, Cat#2897S), ANTI-FLAG (Proteintech, Cat#80010-1-RR).

Lentivirus package, plasmids construction, siRNAs, and transfection

The DNA fragment of LYPLAL1-DT was inserted into pLenti-GIII-EF1α-Luc-2 A-Puro Kan vector (Canada, ABM) and the LYPLAL1-DT shRNA fragment was ligated to the pHBLV-U6-MCS-CMV-ZsGreen-PGK-PURO vector (HANBIO, Shanghai, China). The overexpression lentivirus vector of LYPLAL1-DT, the knockdown and negative controls infected the H446, H446/cDDP and H196 cell lines for 48 h. Subsequently, cells were selected with 2 μg/mL puromycin (Invivogen, Cat#ant-pr-1) for 3 weeks. Furthermore, qRT-PCR was used to examine the overexpression and knockdown efficiency of these cells. The mRFP-GFP-LC3 lentivirus (HANBIO, Shanghai, China) was also infected into the H446 and H446/cDDP cells. The BCL2 expression vector and control vector were purchased from HANBIO and transfected into the cells by using Lipofectamine 3000 (Invitrogen, CA, USA, Cat#L3000015). For the knockdown of LYPLAL1-DT and BCL2, siRNAs or negative control siRNA were transfected via an RNAfit reagent (HANBIO, Shanghai, China), following the manufacturer's instruction. The miR-204-5p mimics, inhibitors and negative controls were also purchased from HANBIO. The sequences of miR-204-5p and siRNAs for LYPLAL1-DT and BCL2 are listed in Table S1.

Western blot

Cells were lysed and then heated in 1×loading buffer (ROBY, Cat#RBU111-1) for 10 min at 99 ℃. The protein samples were separated using SDS-PAGE and transferred onto a nitrocellulose filter membrane (Pall, Cat#51146359). The membranes were blocked with 5% skimmed milk (BD, Cat#232100) for 1 h at room temperature and incubated with primary antibody overnight at 4 °C. Subsequently, the membranes were incubated with secondary antibody for 1 h at room temperature. Protein signals were detected using NcmECL Ultra (NCM Biotech, Cat#P10300) according to the manufacturer's instructions.

RNA extraction and qRT- PCR

Total RNA was extracted using TRIzol (Vazyme, Cat#R401-01) and mRNA was reverse transcribed using 5X All-In-One RT MasterMix (with AccuRT Genomic DNA Removal Kit) (ABM, Cat#G492). qRT-PCR was performed using EvaGreen 2X qPCR MasterMix (ABM, Cat#MasterMix-S). mRNA level was quantified by the 2-ΔΔCt algorithm with β-actin as the normalizer gene, and miRNA expression was normalized to U6. All the primers used are listed in Table S2.

Cell viability assay

For CCK-8 assays, cells were seeded into 96-well plates at a density of 3,000 cells per well for 100 μL. After 12 h of culture, the cells were treated with chemotherapeutic drugs, venetoclax or HCQ, at the indicated concentration for 12 to 72 h. Then, 10 μL of CCK-8 (Gene-Protein-Link, Cat#P04D30X) was added to each well. The cells were then incubated at 37 ℃ for 2 h, and the optical density was measured at 450 nm using a BioTek ELx800 Microplate reader.

Combenefit analysis

Combenefit plots for the combination-dose response of venetoclax with cisplatin and HCQ were generated. H446/cDDP cells were treated with a combination of 2 μg/mL cisplatin and venetoclax (0–160 μM) or a combination of 2 μg/mL cisplatin and HCQ (0–50 μM). Cell viability was then measured by CCK-8 assay after 72 h. Synergy was mapped to drug-dose response using the Loewe model, calculated by SynergyFinder (https://synergyfinder.fimm.fi). Loewe model is based on expected response corresponding to a combination rather than the single drugs with increasing dose. Relative synergy scores are color-coded, where red indicates synergy, white indicates a lack of synergy and green indicates antagonism based on respective synergy scoring. For any doses x_A,

x_B, ...,x_N of drugs *A*,*B*,...,*N*, Loewe synergy score, S_{LOEWE}, is defined as: $S_{LOEWE}= E_{A,\ B,...,N}- E_{LOEWE}$, where E_{LOEWE} should satisfy: $\Sigma_{k = A,\ B,...,N}(x_k f_k^{-1}(E_{LOEWE})) = 1$.

Hoechst-33342 staining for detecting cell apoptosis

Hoechst-33342 staining was performed according to previous report [32]. After cell culture and treatment with chemotherapeutic drugs, the medium was discarded, and the cells were fixed in 4% paraformaldehyde for 15 min. Subsequently, 200 μL of 100 μg/mL Hoechst-33342 (Solarbio, Cat#C0021) was added to cover the cells, and incubated for 15 min in the dark. Afterwards, cells were gently washed three times with phosphate buffer saline (PBS) to prevent the loss of apoptotic cells, and cellular morphology was observed using fluorescence microscopy. Cells showing intensely condensed nuclei and/or nuclei fragments were considered apoptotic.

Annexin V-FITC/PI apoptosis detection

After the cell treatment, both floating and adherent cells were collected together. Using Annexin V-FITC/PI Apoptosis Detection Kit (Vazyme, Nanjing, China, Cat#A211-01) following the manufacturer's instructions, the cells were washed with PBS and resuspended in 100 μL binding buffer (1×10^5 cells per group). Next, 5 μL Annexin V-FITC and 5 μL propidium iodide staining solution were added to each tube. After mixing, cells were incubated at 37 ℃ for 10 min in the dark. Subsequently, an additional 400 μL of binding buffer was added to each tube, and the flow cytometry analysis was carried out using BD LSRFortessa flow cytometry.

RNA immunoprecipitation (RIP) assay

RIP analysis was performed using Magna RIPTM RNA-Binding Protein Immunoprecipitation Kit (Millipore, Billerica, MA, USA, Cat#17–700) following the manufacturer's protocol. H446 and H446/cDDP cell lysates were incubated with magnetic beads conjugated with anti-BECN1, anti-PIK3C3 or Ago2 antibody (CST, USA) and IgG antibody at 4 °C for 6 h. The magnetic beads were washed 4–6 times with RIP washing buffer to remove non-specific adsorption as much as possible. The protein-RNA complex with magnetic beads were digested with 0.5 mg/mL proteinase K at 55 ℃ to purified RNA and eluted RNA from magnetic beads. Finally, the extracted RNA was reverse transcribed and analyzed by qRT-PCR.

Dual-luciferase reporter assay

The LYPLAL1-DT sequence, containing 2577 bp, and the 3'-UTR of BCL2, containing 5279 bp, were cloned and inserted into the psi-check2 plasmid. The miR-204-5p target site mutations of LYPLAL1-DT and BCL2 3'-UTR luciferase reporter plasmids were generated by HANBIO (Shanghai, China). H446 and H446/cDDP cells were seeded in a 6-well plate and co-transfected with the constructed recombinant plasmids (2 μg/well) or control plasmids along with miR-204-5p mimics. After 48 h, luciferase and Renilla luciferase activities were measured separately using the Dual-Luciferase Reporter Assay Kit, following the manufacturer's instruction (Vazyme, Cat#DL101-01). The ratio of renilla luciferase luminescence to firefly luciferase luminescence was then calculated.

Determination of mitochondrial membrane potential

The enhanced mitochondrial membrane potential assay kit with JC-1 (Beyotime, Cat#C2003S) was used. JC-1 was diluted by adding 1 mL JC-1 dyeing buffer per 5 μL JC-1 (200×). The cells were inoculated in confocal small dish. Removed the dish after drug treatment and cleaned with PBS. Next, 1 mL of cell culture medium and 1 mL of JC-1 dyeing solution were added and incubate at 37 °C for 20 min, and then removed the supernatant and washed the cell with JC-1 staining buffer. Finally, added 2 mL of cell culture medium and observed under laser confocal microscope. Set excitation wavelength to 490 nm and the emission wavelength to 530 nm to detect JC-1 monomers. Set excitation wavelength to 525 nm and the emission wavelength to 590 nm to detect JC-1 aggregates.

Determination of caspase activity

The activity of caspase-3 was measured using the Caspase3 Activity Detection Kit (NJJCBIO, Cat#G015-1). Briefly, cells were collected after drug treatment. Next, 50 μL of lysis buffer with 1% DTT was added for 30 min, followed by the addition of 50 μL 2×reaction mixture, 5 μL acety-Asp-Glu-Val-Asp p-nitroanilide (Ac-DEVD-pNA), and overnight incubation at 37 °C. The related caspase activity was quantified at 450 nm using a BioTek ELx800 Microplate reader.

Colony formation assay

H446/cDDP cells were seeded into 6-well plates with 200 cells per well. After 12 h of incubation at 37 °C, the cells were treated with cisplatin for 3 days every week, venetoclax and HCQ for 14 days, during which the medium was changed every 3 days. The cells were fixed with 4% paraformaldehyde fix solution (APPLYGEN, Cat#B1057) for 30 min and strained with 0.01% crystal violet (APPLYGEN, Cat#B1087). Images were obtained, and the number of colonies was counted.

Transmission electron microscopy (TEM)

Cells were collected and fixed in 2.5% glutaraldehyde for 30 min at room temperature. Subsequently, the fixed cells underwent dehydrated using a graded ethanol series. A graded series of acetone was applied to the samples, which were then embedded in Epon. The embedding

blocks were sliced at a thickness of 50–70 nm for follow-up observation. Electron microscopy was performed using the HT7700 transmission electron microscope (HITACHI, Japan).

Immunofluorescence and confocal microscopy

Cells were seeded into glass bottom cell culture dishes (NEST, Cat#801001) at 2×10^5 cells per well. After treatment with the indicated chemotherapeutic drugs for a specific duration, cells were washed with PBS and fixed in 4% paraformaldehyde for 30 min. Subsequently, the cells were blocked for 1 h with 5% BSA, followed by overnight incubation with a primary antibody at 4 ℃. The next day, cells were washed with PBS three times, and then incubated with secondary antibodies for 1 h at room temperature. Finally, 1 mg/mL Hoechst-33342 was added to stain nuclei, and the cells were photographed under a fluorescence microscope.

IF/FISH

Fluorescence-conjugated probes, designed and purchased from GenePharma (Shanghai, China), were used for IF/FISH. Cells treated with chemotherapeutic drugs were hybridized to fluorescence-conjugated probes according to the manufacturer's instructions (GenePharma, Shanghai, China). The probe sequences were as follows: LYPLAL1-DT, 5′-GGGTTTCGTCGAGGCTT GGGTCGG-3′. Anti-BECN1, anti-PIK3C3 and secondary antibodies were added for immunofluorescence. The samples were counterstained with Hoechst and observed by confocal microscopy.

Autophagic flux analysis

To analyze autophagic flux, cells were stably transfected with mRFP-GFP-LC3 Lentivirus (HANBIO, Shanghai, China) following the manufacturer's instructions. Subsequently, the cells were treated with chemotherapy drugs for the designated time, and the expression levels of GFP and mRFP were observed using confocal fluorescence microscopy.

Co-immunoprecipitation (Co-IP)

For Co-IP, cells were lysed in RIPA buffer on ice for 30 min, and the supernatants were collected by centrifugation at 4 °C and 15,000 g for 15 min. Discard the precipitate, the cleared protein lysates were then incubated overnight at 4 °C with magnetic beads bound with primary antibody. The following day, the beads were collected, washed 5 times with 0.5 mL washing buffer and SDS loading buffer was added. The samples were denatured at 99 °C for 10 min. Finally, the supernatants were collected, stored at -80 °C, or immediately analyzed by Western blot.

Immunohistochemistry (IHC)

For immunohistochemical study, after dehydration and antigen repair, tissue sections were blocked using 10% BSA, then incubated overnight at 4 °C with primary antibodies (1: 200 dilution) against BCL2 and BECN1. Subsequently, the sections were incubated with a secondary antibody (1: 200 dilution) at room temperature for 1 h. IHC staining was visualized using the DAB Immunohistochemistry Color Development Kit (ZSGB-BIO, Cat#ZLI-9019) according to the manufacturer's instructions. After washing 3 times and counterstaining with hematoxylin, slides were dehydrated with sequential ethanol washes and sealed. The expression of BCL2 and p62 was analyzed and evaluated using optical microscopy.

Subcutaneous xenograft experiments and patient-derived xenograft studies

For subcutaneous xenograft studies, H446 cells (stably overexpressing LYPLAL1-DT or an empty vector) or H446/cDDP cells (2×10^6 / 200 μL) were inoculated subcutaneously into 4- to 6-week-old NTG male mice (SiPeiFu, Beijing, China). For patient-derived xenograft studies, NTG mice were obtained from IDMO (Beijing, China). Cryopreserved PDX tumors (No. A7391, No.21031902, No.20090907, No.19111114) were implanted subcutaneously into the mice. Subsequently, four replicates were randomly selected per group for the following experiments. Mice were treated with cDDP, PTX, VP-16, venetoclax and HCQ after the tumor volume reaches 50–100 mm^3. cDDP (1.5 mg/kg), VP-16 (5 mg/kg) and PTX (5 mg/kg) were administered via intraperitoneal injection (i.p.) once a week. Venetoclax (50 mg/kg) was administered by oral gavage (i.g.) and HCQ (15 mg/kg) was given by intraperitoneal injection (i.p.) every 2 days. Treatment study continued for 2–3 weeks. The lengths and widths of tumors were measured every two days until the endpoint. Tumor volume was calculated as height×width×width×0.5. The studies were approved by the Committee on the Ethics of Animal Experiments of Capital Medical University (No. AEEI-2019-089).

Statistical analysis

Graphing and Statistical analysis were performed using Graphpad Prism. Data were presented as mean±SEM, and statistical significance was determined by Student's t-test (t-test) or two-way ANOVA, as indicated in the figure legend. The sample size (n) is also reported in the figure legend for each experiment, with 'n' representing the number of identically treated replicates. All tests were two-tailed, and P values <0.05 were considered statistically significant.

Results

LYPLAL1-DT contributes to multi-drug resistance in SCLC

Our previous studies indicated that lncRNA LYPLAL1-DT was closely correlated with SCLC progression [32]. To investigate the role of LYPLAL1-DT in the chemotherapy sensitivity of SCLC, we first detected the circulating level of LYPLAL1-DT, which were remarkably higher in the serum of chemoresistant patients ($n=9$) compared to chemosensitive patients ($n=8$). We also found that higher LYPLAL1-DT levels were associated with poor progression-free survival (PFS) (Fig. 1A, S1A). To explore this notion, we then established cisplatin (cDDP) resistant SCLC cell line H446/cDDP or H196/cDDP, etoposide (VP-16) resistant cell line H446/VP-16 or H196/VP-16 and paclitaxel (PTX) resistant cell line H446/PTX or H196/PTX cells (Fig. S1B-C). Intriguingly, we found that the LYPLAL1-DT level was much higher in chemo-resistant cell lines than the parental cells ($p<0.001$, Fig. 1B-C). Furthermore, both H446 and H196 cells treated with chemotherapeutic drugs (cDDP, VP-16, or PTX) showed an upregulation of LYPLAL1-DT expression in both a dose- and time-dependent manner (Fig. 1D-G, S1D-E). Except for the stably overexpressed LYPLAL1-DT of H446 cells as previously reported [32], we stably knocked it down in H446/cDDP and H196 cell lines via lentivirus transduction (Fig. S1F-G). Cell viability assay showed that overexpression of LYPLAL1-DT promoted the chemoresistance of H446, and the IC50 value increased significantly compared to control cells (Fig. 1H-J, S1H). Data also revealed that the down-regulation of LYPLAL1-DT increased the sensitivity of H446/cDDP and H196 to cisplatin, VP-16, and PTX (Fig. 1K, S1I). These data indicates that LYPLAL1-DT may play important roles in SCLC multiple-chemoresistance.

LYPLAL1-DT reduces the chemosensitivity of SCLC cells by inhibiting apoptosis

The cytotoxicity of antineoplastic drugs mainly depends on their ability to induce cell death. Deregulation of apoptosis is a fundamental characteristic of cancer cells that is involved in both tumorigenesis and multi-drug resistance [33]. To investigate whether LYPLAL1-DT participates in the regulation of apoptosis, we detected cell apoptosis by Hoechst staining, flow cytometry, and caspase 3 level analysis. The data revealed that after treatment with chemotherapeutic drugs, the ratio of apoptosis cells with typical features (nuclei condensation) decreased remarkably in the LYPLAL1-DT overexpressing group compared to the control group, while the opposite trend was observed in LYPLAL1-DT knockdown cells (Fig. 2A-B, S2A). To define the apoptosis pathway adopted by tumor cells under chemotherapy, we detected the expression of caspase 3. Compared with control cells, caspase 3 activity was lower in LYPLAL1-DT overexpressing cells but higher in cells with LYPLAL1-DT knockdown under cDDP, VP-16, or PTX treatment (Figs. 2C-D, S2B-C). Flow cytometry confirmed that LYPLAL1-DT overexpression decreased the sensitivity of H446 cells to chemotherapeutic drugs, as indicated by the reduced number of annexin V-PI-positive cells (Fig. 2E-F). Additionally, Cytochrome C released into the cytoplasm was much lower in LYPLAL1-DT-overexpressed H446 cells than in control cells (Fig. 2G); JC-1 fluorescence staining showed that the green fluorescence intensity of LYPLAL1-DT-overexpressed H446 cells was significantly lower than that of the control group with cDDP treatment, indicated mitochondrial membrane potentials (MMP) were reduced in LYPLAL1-DT-overexpressed H446 cells (Fig. 2H). All the results above demonstrate that LYPLAL1-DT decreases chemosensitivity of SCLC by inhibiting the mitochondrial apoptotic pathway.

LYPLAL1-DT reduces the chemosensitivity by promoting autophagy

Increasing evidence reveals that autophagy plays a central role in chemoresistance of tumor cells, enabling them to survive chemotherapy and eventually leading to relapse. Our previous results also showed that autophagy increased in H446/cDDP cells [26]. To determine if there is correlation between LYPLAL1-DT and autophagy under various chemotherapeutic drug treatments, we detected the expression levels of LC3 and p62/SQSTM1, indicators of autophagosome formation, in LYPLAL1-DT overexpressed H446, LYPLAL1-DT knockdown H446/cDDP and H196 cells by Western blot. It was observed that LC3-II levels were positively correlated with the expression of LYPLAL1-DT, while p62 showed a negative correlation (Fig. 3A-B, S3A-B).

To further confirm the roles LYPLAL1-DT played in autophagy, we used mRFP-GFP-targeted LC3 fluorescence to visualized autophagy flux. As showed in Fig. 3C-D and S3C-D, LYPLAL1-DT overexpression increased the level of autolysosomes (red dots) after chemotherapeutic drugs treatment and was blocked in siRNA-transfected cells after cisplatin treatment comparing with control cells. Furthermore, transmission election microscopy (TEM) showed that the number of intracellular autophagosomes significantly increased with LYPLAL1-DT overexpression (Fig. 3E-F). These results suggest that LYPLAL1-DT participates in the modulation of both autophagy and apoptosis under chemotherapeutic exposure.

LYPLAL1-DT upregulates BCL2 expression by direct targeting miR-204-5p

One of the ways lncRNA functions is by acting as a competing endogenous RNA (ceRNA). ceRNAs can sequester miRNAs, thereby protecting their target RNAs from

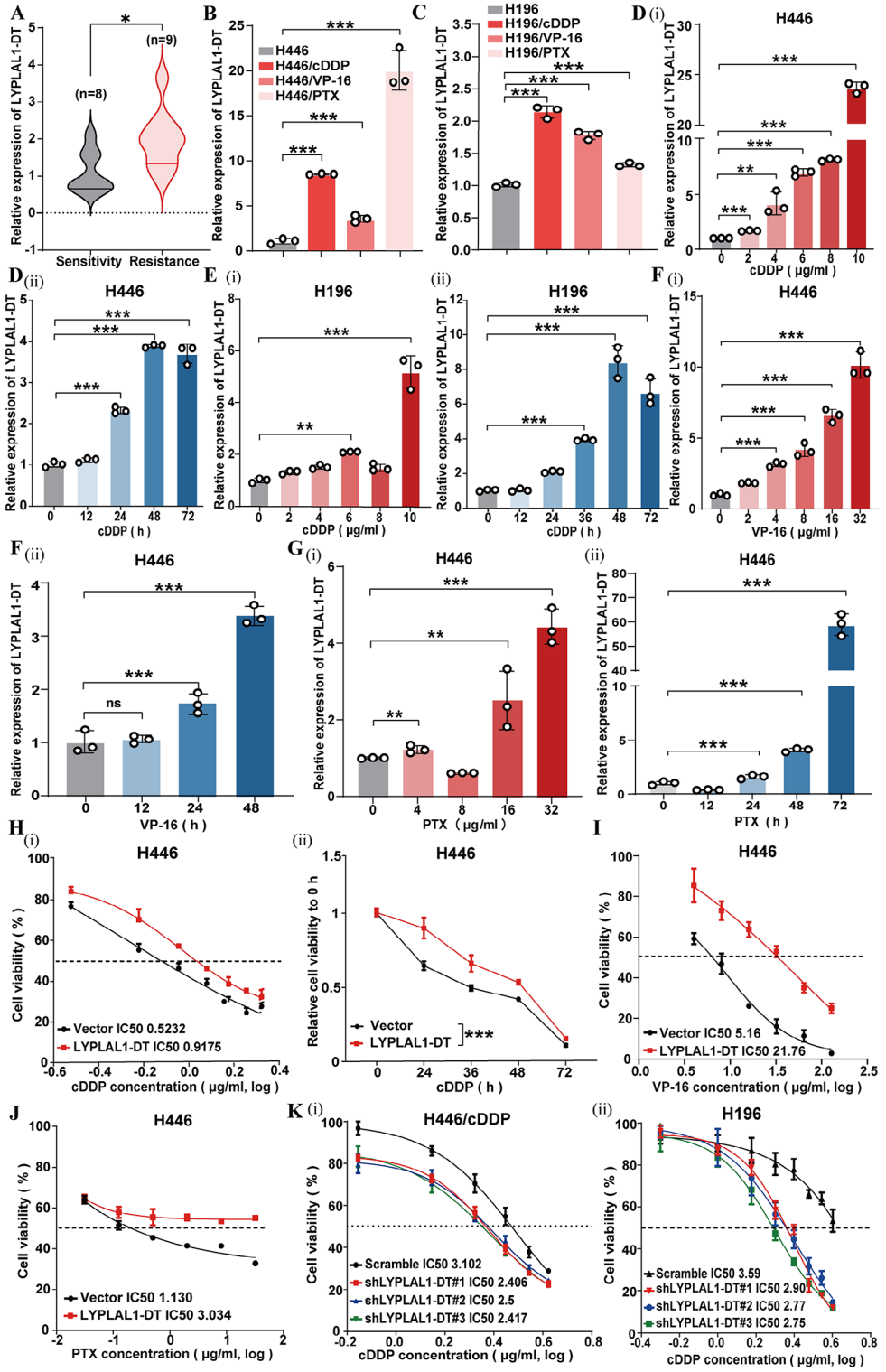

Fig. 1 LYPLAL1-DT contributes to multi-drug resistance of SCLC. **(A)** Comparing the expression level of LYPLAL1- DT in the serum of chemoresistant patients ($n=9$) and chemosensitive patients ($n=8$) by qRT-PCR. **(B)** Comparing the expression of LYPLAL1-DT in H446/cDDP, H446/VP-16 and H446/PTX with parental cells. **(C)** Comparing the expression of LYPLAL1-DT in H196/cDDP, H196/VP-16 and H196/PTX with parental cells. The expression level of LYPLAL1-DT in H446 **(D)** or H196 cells **(E)** under cDDP treatment at different times or concentrations. The expression level of LYPLAL1-DT in H446 cells under VP-16 **(F)** or PTX **(G)** treatment at different times or concentrations. **(H-J)** Comparing the cell viability of LYPLAL1-DT overexpressed H446 cells with their control cells under cDDP, VP-16 or PTX treatment at various time or concentration. **(K)** Comparing the cell viability of LYPLAL1-DT knockdown H446/cDDP cells or H196 cells with their control cells under cDDP treatment at various time or concentration. (*, $P<0.05$; **, $P<0.01$; ***, $P<0.001$)

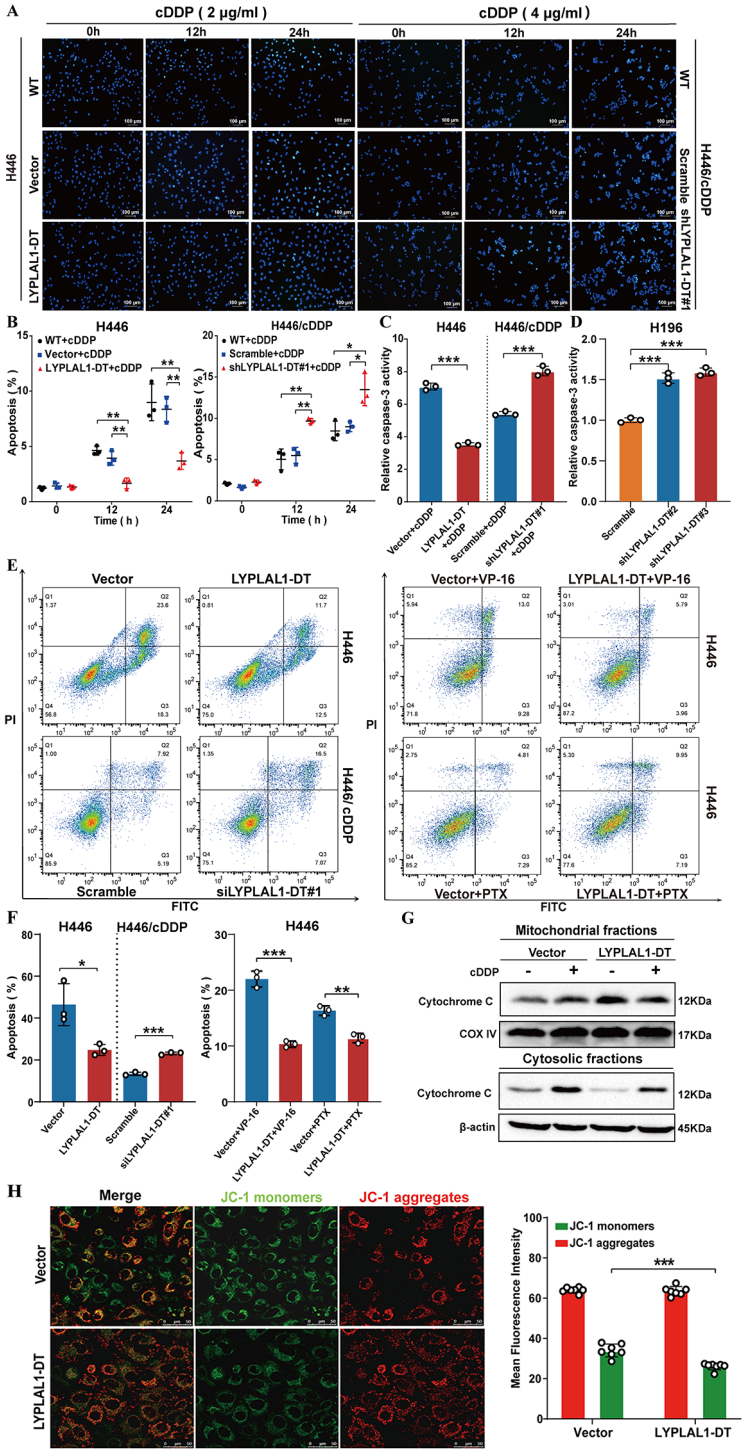

Fig. 2 LYPLAL1-DT reduces chemosensitivity of SCLC cells by inhibiting apoptosis. **(A-B)** H446 and H446/cDDP cell lines transfected with the indicated vectors or LYPLAL1-DT or shLYPLAL1-DT and treated with cDDP at different times as determined by Hochest staining assay. The number of positive cells was quantified. **(C-D)** Comparing the relative caspase-3 activity of LYPLAL1-DT overexpression or knockdown cells and their control cells by caspase-3 activity assay kit. **(E-F)** The apoptosis rates of H446 cells transfected with vectors or LYPLAL1-DT, and H446/cDDP cells transfected with scramble or LYPLAL1-DT siRNA were analyzed by Flow cytometry under cDDP, VP-16, or PTX treatment. The number of Annexin V-PI-positive cells was quantified. **(G)** The expression level of cytochrome C in mitochondrial fractions or cytosolic fraction of H446 cells with or without cDDP treatment. **(H)** JC-1 fluorescence staining was analyzed in LYPLAL1-DT-overexpressed H446 cells and the control group with cDDP treatment (*, $P < 0.05$; **, $P < 0.01$; ***, $P < 0.001$)

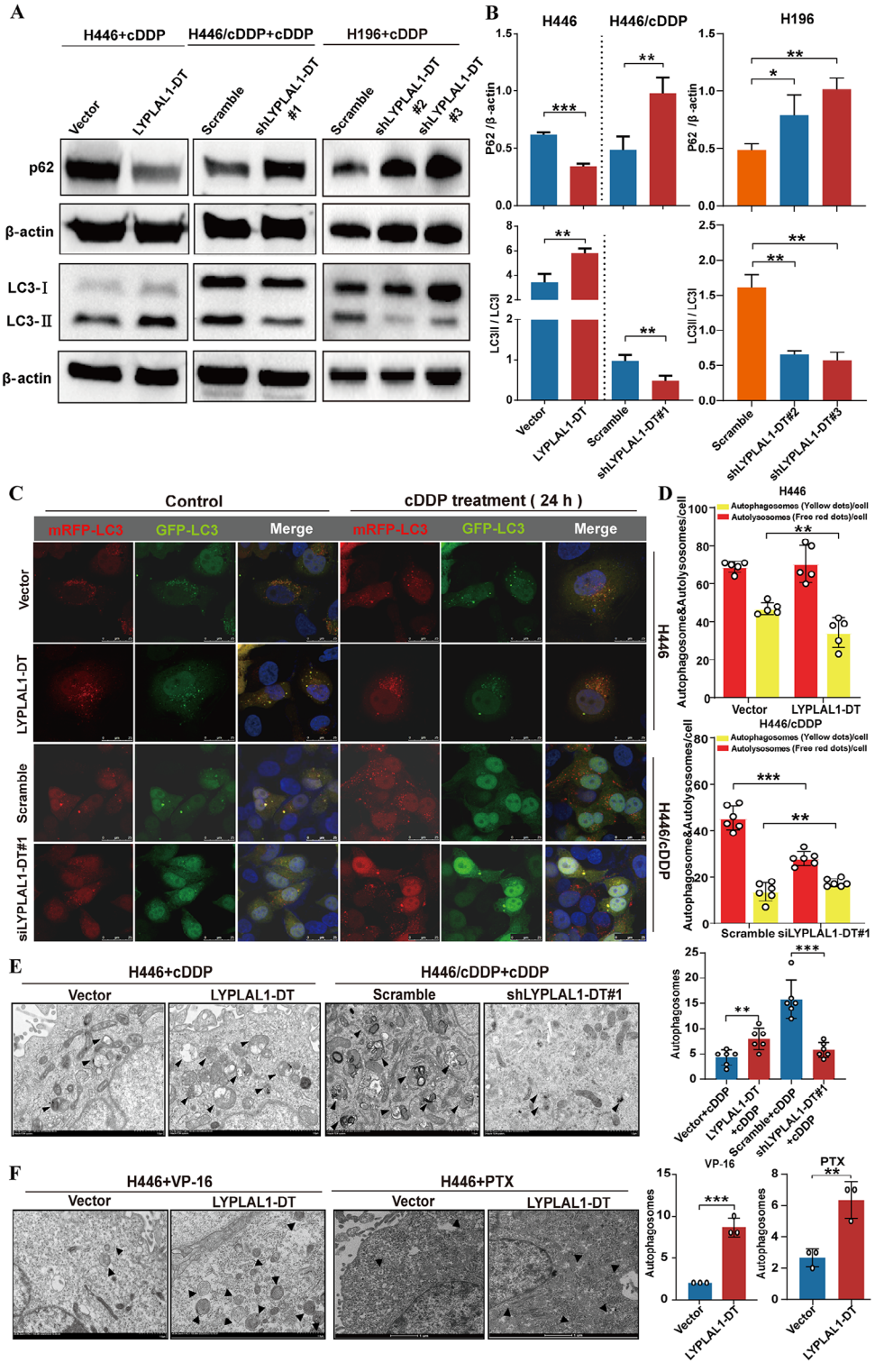

Fig. 3 LYPLAL1-DT reduces the chemosensitivity of SCLC cells by promoting autophagy. **(A-B)** H446 cells transfected with vectors or LYPLAL1-DT and H446/cDDP or H196 cells transfected with scramble or shLYPLAL1-DT, were treated with cDDP. The expression of LC3 and p62 were analyzed by Western blot. The expression ratio of p62/β-actin and LC3-II/LC3-I were determined. **(C-D)** LYPLAL1-DT overexpressing cells and LYPLAL1-DT knockdown cells were treated with cDDP and the autophagy flux were visualized by mRFP-GFP-targeted LC3 fluorescence. The number of autophagosomes and autolysosomes was quantified. **(E-F)** Transmission electron microscopy showed the changes of autophagosomes (as indicated by the arrows) in LYPLAL1-DT-overexpressing H446 or -knockdown H446/cDDP cells under cDDP, VP-16, or PTX treatment (*, $P < 0.05$; **, $P < 0.01$; ***, $P < 0.001$)

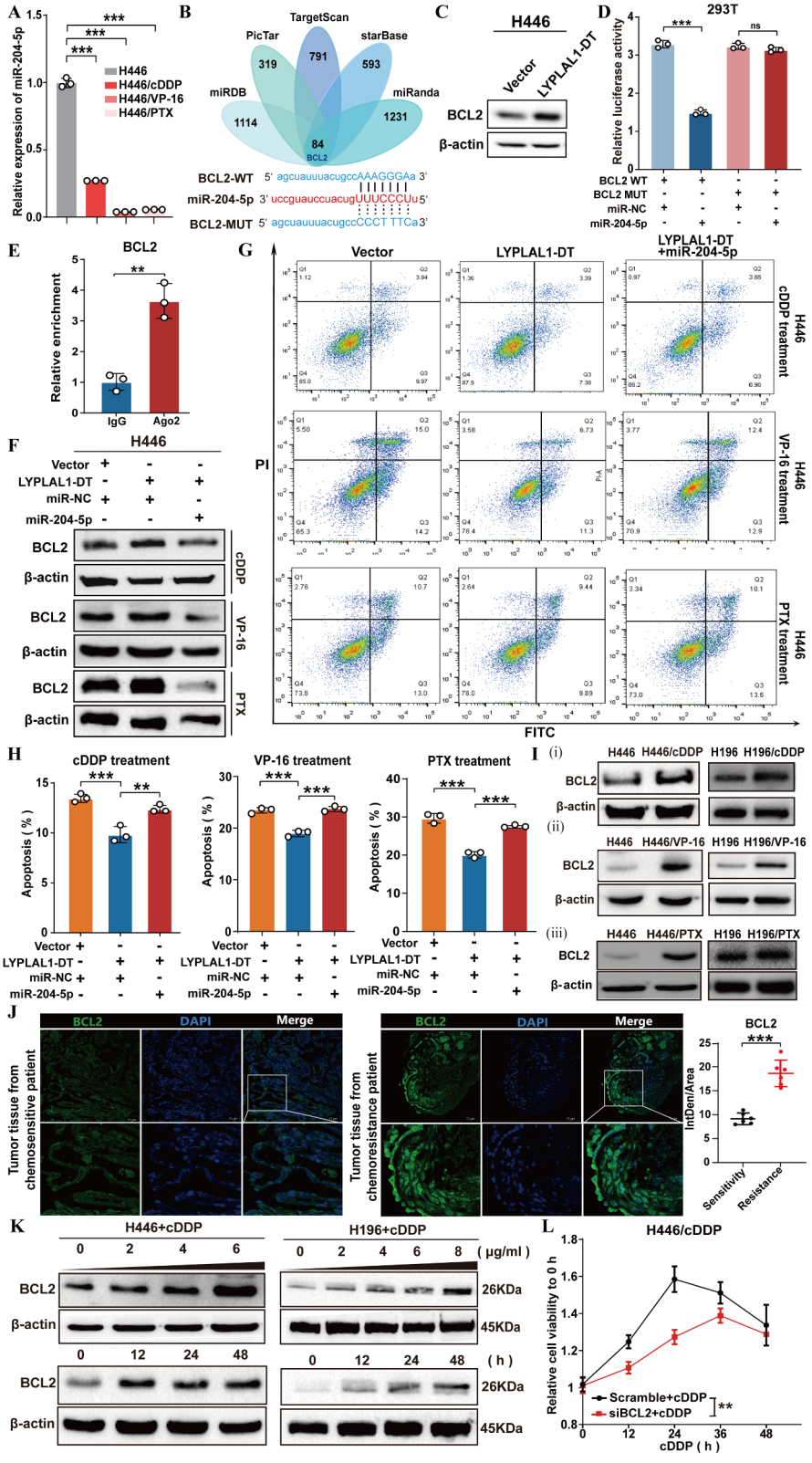

Fig. 4 (See legend on next page.)

(See figure on previous page.)

Fig. 4 LYPLAL1-DT/BCL2/miR-204-5p axis is involved in the chemoresistance of SCLC cells. **(A)** The expression level of miR-204-5p in H446/cDDP, H446/VP-16, H446/PTX and their control cells. **(B)** Five bioinformatics algorithms were used to predict the potential regulatory targets of miR-204-5p and the sequences of miR-204-5p, BCL2-WT and BCL2-MUT. **(C)** Western blot showed the expression level of BCL2 in LYPLAL1-DT-overexpressing H446 cells and control cells. **(D)** Dual-luciferase reporter assay indicated the luciferase activity in 293T cells co-transfected with WT or mutant BCL2 and miR-204-5p mimic or miRNA-NC. **(E)** RIP assay showed the binding possibilities of BCL2 with Ago2 or IgG. **(F)** Western blot showed the expression of BCL2 in LYPLAL1-DT-overexpressing H446 cells co-transfected with miR-204-5p mimics or miRNA-NC with cDDP, VP-16, or PTX treatment. **(G-H)** Flow cytometry analysis of apoptosis in LYPLAL1-DT-overexpressing H446 cells co-transfected with miR-204-5p mimics prior to the stimulation of cDDP, VP-16, or PTX treatment for 24 h. **(I)** Western blot showed the expression level of BCL2 in cDDP-, VP-16-, PTX-resistant H446 or H196 cells. **(J)** Immunofluorescence staining of BCL2 in the sections of tumor tissues from drug-resistant ($n=6$) and drug-sensitive ($n=6$) groups. **(K)** The expression level of BCL2 in H446 and H196 cells were detected under cDDP treatment at different times and concentrations. **(L)** The relative cell viability to 0 h of H446/cDDP cells transfected with siBCL2 or scramble were analyzed by CCK-8 assay under cDDP treatment at different times (*, $P<0.05$; **, $P<0.01$; ***, $P<0.001$)

repression. Our previous study illustrated that miR-204-5p is one the regulatory microRNAs of LYPLAL1-DT [32]. By RIP assay, we confirmed the enrichment of LYPLAL1-DT in miR-204-5p/ago2 complex (Fig. S4A). To determine whether LYPLAL1-DT/miR-204-5p axis plays a role in response to chemotherapeutic drugs treatment, we assessed the expression level of miR-204-5p under various conditions. It showed that its expression decreased significantly in H446/cDDP, H446/VP-16, and H446/PTX, as well as in H446 after cDDP, VP-16, or PTX treatment in both a concentration- and time-dependent manner (Fig. 4A, S4B-C). Simultaneous overexpression of LYPLAL1-DT with miR-204-5p mimics significantly decreased cell viability compared to that in LYPLAL1-DT-overexpressed cells in a time-dependent manner, while miR-204-5p inhibitors increased the IC50 value and restored the decreased cell viability caused by LYPLAL1-DT knockdown (Fig. S4D-G).

To further explore the target genes of miR-204-5p, we used 5 bioinformatics algorithms (miRanda, PicTar, TargetScan, miRDB and starBase) to predict its potential regulatory targets. Among the upregulated genes in H446/cDDP, BCL2, one of the key arbiters of apoptosis, emerged in the overlapping gene pool of the bioinformatic algorithms (Fig. 4B). Overexpression of LYPLAL1-DT significantly increased the expression of BCL2 (Fig. 4C). To verify whether miR-204-5p targets the 3'-UTR of BCL2, we constructed luciferase reporters containing BCL2 3'-UTR (WT) or with binding site mutation (MUT). Co-transfection of the miR-204-5p mimics significantly reduced the luciferase activity of BCL2 in the cells transfected with BCL2 WT, but not in those transfected with MUT BCL2 3'-UTR (Fig. 4D). The RNA immunoprecipitation (RIP) assay indicated that BCL2 binds to the RISC complex formed by LYPLAL1-DT, miR-204-5p and Ago2 (Fig. 4E). Furthermore, a rescue assay was performed to clarify the regulatory axis of LYPLAL1-DT/miR-204-5p/BCL2 in SCLC MDR. Overexpression of LYPLAL1-DT significantly increased the expression of BCL2, while the miR-204-5p mimics partially rescued the upregulation (Fig. 4F). Overexpression of miR-204-5p mimics significantly ameliorate the apoptosis inhibition induced by LYPLAL1-DT (Fig. 4G-H). Moreover, Western blot and qRT-PCR unveiled the significant upregulation of BCL2 in cDDP-, VP-16- and PTX-resistant cell lines (Fig. 4I, S4H). The similar results were observed in the tumor sections of chemotherapy-resistant patients (Fig. 4J). While under chemodrug treatment, its increasement is concentration- and time-dependent (Fig. 4K, S4I-J). CCK-8 assay showed the cell viability and IC50 of H446/cDDP cells decreased remarkably when silencing BCL2 under cDDP treatment (Fig. 4L, S4K).

Taken together, our data has verified LYPLAL1-DT upregulates BCL2 expression by suppressing miR-204-5p, which contributes to the MDR of SCLC cells.

LYPLAL1-DT facilitates the assembly of the BECN1/PIK3C3 complex

Beclin1(BECN1) is a protein that plays a crucial role in the initiation of autophagy by forming a complex with PIK3C3, which is essential for the formation of the autophagosome. Our data showed that the expression level of BECN1 increased significantly after cDDP, VP-16 or PTX treatment, both in a concentration- and time-dependent manner (Fig. 5A-B). This was proved in H446/cDDP, H446/VP-16 and H446/PTX cell lines by Western blot and immunofluorescence of tumor sections (Fig. 5C-D). However, the activity of BECN1 is negatively regulated by BCL2, which binds the BH3 domain of BECN1. This traditional pathway is contradicted to what we observed that the autophagy increased in chemoresistant cells despite of the upregulation of BCL2. The observation prompts us to explore the underlying mechanism involved in the enhancement of autophagy. We found that the interaction of BCL2 and BECN1 decreased sharply with the increase of cDDP concentration in cDDP-resistant H446 cells by co-IP assay (Fig. S5A). Interestingly, upregulation of LYPLAL1-DT also suppressed the interaction of BCL2 and BECN1 and prompted the assembly of class III PI3K complex (Fig. S5B). With the help of RNA-protein interaction prediction tool RPISeq (RPISeq, http://pridb.gdcb.iastate.edu//RPISeq/), we predicted that LYPLAL1-DT is probably involved in the assembly of the BECN1/PIK3C3 complex (Fig. S5D-E). IF/FISH indicated the colocalization of

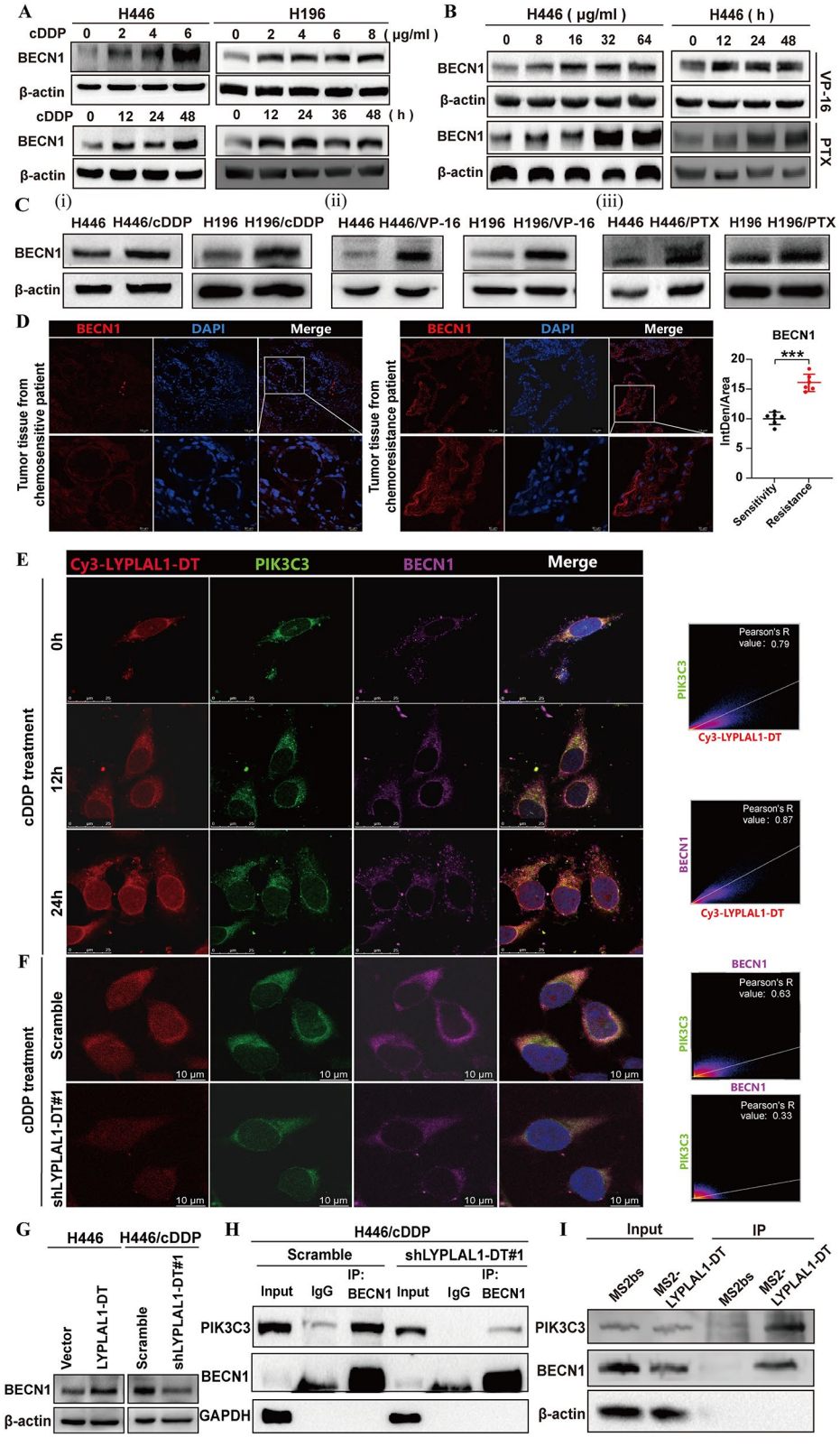

Fig. 5 (See legend on next page.)

(See figure on previous page.)

Fig. 5 LYPLAL1-DT facilitates the assembly of the core players of autophagy, BECN1/PIK3C3 complex. **(A-B)** The expression level of BECN1 of H446 or H196 cells with cDDP, VP-16 or PTX treatment at different times and concentrations. **(C)** The expression level of BECN1 in cDDP-, VP-16- and PTX-resistant H446 or H196 cells. **(D)** The sections of tumor tissues from chemosensitive patients ($n=6$) and chemoresistant patients ($n=6$) patients were stained with BECN1. **(E)** IF/FISH images showing the colocalization of LYPLAL1-DT and BECN1, PIK3C3 in H446/cDDP cells with cDDP treatment by fluorescence confocal microscopy. **(F)** IF/FISH images showing the colocalization of LYPLAL1-DT and BECN1, PIK3C3 in H446/cDDP cells transfected with scramble or LYPLAL1-DT shRNA with cDDP treatment by fluorescence confocal microscopy. **(G)** Western blot showed the expression level of BECN1 in LYPLAL1-DT-overexpressing H446 cells or LYPLAL1-DT-knockdown H446/cDDP cells. **(H)** H446/cDDP cells were transfected with scramble or shLYPLAL1-DT, and the coupling between BECN1 and PIK3C3 was shown by immunoprecipitation. (**I**) RNA pull-down assay confirmed the interaction of LYPLAL1-DT and BECN1/PIK3C3 complex (**, $P<0.01$; ***, $P<0.001$)

LYPLAL1-DT with BECN1 and PIK3C3 in H446/cDDP cells by fluorescence confocal microscopy (Fig. 5E), while LYPLAL1-DT inhibition impaired the interaction of BECN1 and PIK3C3 (Fig. 5F). RIP indicated that LYPLAL1-DT was significantly enriched by BECN1 and PIK3C3 compared with IgG (Fig. S5C). Furthermore, overexpression of LYPLAL1-DT significantly increased the expression of BCL2 (Fig. 5G). co-IP also showed that the BECN1/PIK3C3 complex was impaired by LYPLAL1-DT knockdown (Fig. 5H). To determine whether LYPLAL1-DT directly binds to BECN1 and PIK3C3, we transfected an MS2-tagged LYPLAL1-DT plasmid into H446 cells (Fig. 5I) and found that LYPLAL1-DT may act as a scaffold involved in the assembly of BECN1/PIK3C3 complex. These data provided the evidence that LYPLAL1-DT is involved in the assembly of the BECN1/PIK3C3 complex to promote autophagy in chemoresistant SCLC.

Combinations of cDDP/VP-16/PTX, venetoclax and HCQ enhance cell death in chemoresistant SCLC in vitro and in vivo

When unveiling the roles of apoptosis and autophagy in chemotherapy resistant SCLC cells, we attempted to use venetoclax (an antagonist of the antiapoptotic protein BCL2) and hydroxychloroquine (HCQ, an autophagy inhibitor) to improve the treatment of SCLC cells. A combenefit analysis revealed that the triple combination of cDDP + venetoclax+HCQ resulted in a dramatic reduction in cell growth compared to other options (cDDP+venetoclax or cDDP+HCQ) and the sensitivity of H446/cDDP cells to cDDP was significantly restored when combined with venetoclax and HCQ (Fig. 6A-C). The Loewe synergy score reached to 13.703 in H446/cDDP cells and 12.679 in H196/cDDP cells. The colony formation assay demonstrated the remarkable effectiveness of the triple combination when treated with various medications over a 14-day period (Fig. 6D). The caspase-3 activity increased sharply in triple combination (Fig. 6E), and the autophagy level induced by venetoclax was suppressed remarkably through HCQ treatment (Fig. 6F, S6A). It showed similar trends when we extended the triple combination strategy to cDDP, VP-16 or PTX treatment, chemotherapy resistant H196 cells also exhibited excellent response to triple combination drugs (Fig. 6G-H, I-K, S6B-C).

Additionally, we established cell line-derived xenograft (CDX) mice models by subcutaneously injecting H446/cDDP, LYPLAL1-DT-overexpressed H446 cells or the empty vector control cells, and treated with a myriad combination of chemotherapeutic drugs. It indicated that the triple combination remarkably alleviated chemoresistance in H446/cDDP-derived xenograft mice models (Fig. 7A-B). The expression of BCL2 and p62 in tumor tissues were accessed by immunohistochemistry (Fig. S7A). This phenomenon coincided with VP-16 and PTX treated mouse models (Fig. 7C-D, S7B-C). Moreover, mice exhibited similar body weight through drug treatment (Fig. S7D).

To further evaluate the therapeutic potential of this triple combination, we utilized patient-derived xenografts (PDX) from four patients (No.A7391, No.21031902, No.20090907, No.19111114). The expression level of LYPLAL1-DT in the first three examples is much higher than that in the last one (Fig. S8A). Data showed that venetoclax and HCQ significantly increase cDDP-, VP-16 or PTX-induced cell death in the three samples with high LYPLAL1-DT expression, while showing little responsiveness in xenografts with low LYPLAL1-DT expression (Fig. 8A-E). Immunohistochemistry showed a remarkably reduced expression level of BCL2 and increased p62 in tumor tissues under triple-drug treatment (Fig. S8B-E). However, it was unapparent in the No.19111114-derived tumor tissues with relatively lower expression of LYPLAL1-DT (Fig. S8H).

To further assess the safety of the triple therapy regimen, we compared liver and kidney damage across different treatment approaches through histological analysis (Fig. S8F-G, S8I). Also, we measured various serum indicators of liver function and kidney function (Fig. S8J). The results showed no significant differences between all the groups ($p>0.05$), indicating the promising prospects of the triple therapy regimen in clinical application.

Discussion

SCLC is an aggressive malignancy with early dissemination and an extremely poor prognosis. One of the hallmarks of SCLC is that acquired resistance to cytotoxic develops rapidly and occurs in nearly all patients with

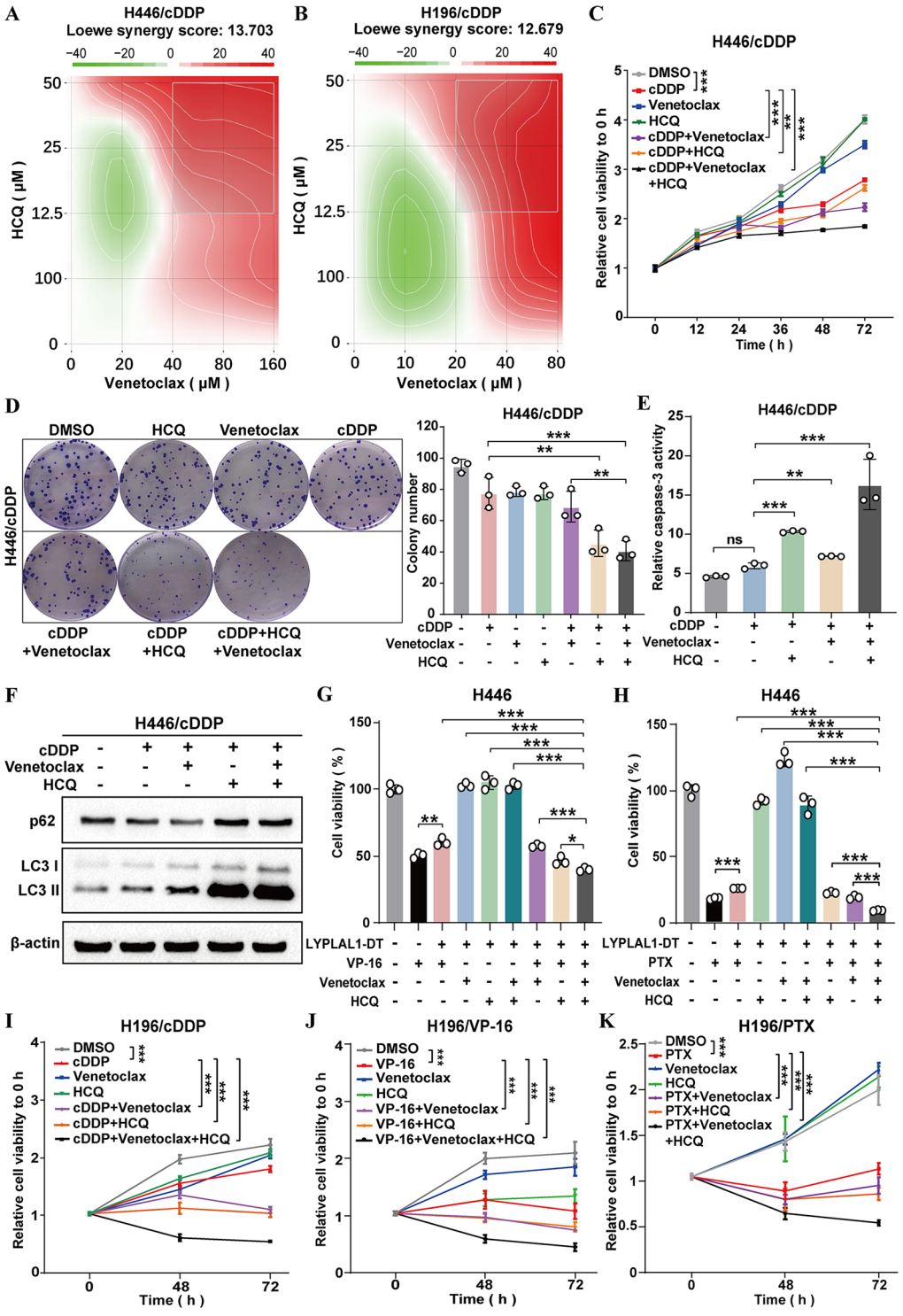

Fig. 6 Combinations of cDDP/VP-16/PTX, venetoclax and HCQ enhance cell death in chemoresistant SCLC in vitro. **(A-B)** The combenefit analysis was performed to identify the synergistic interaction of drug combinations (cDDP + venetoclax, cDDP + HCQ, or cDDP + venetoclax + HCQ) in H446/cDDP or H196/cDDP cells. **(C)** CCK-8 assay was used to detect the relative cell viability of H446/cDDP under various drug combinations indicated above. **(D)** The colony formation assay demonstrated and analyzed the effectiveness of various medications over a 14-day period. **(E)** The caspase-3 activity of H446/cDDP cells under various medications treatment. **(F)** Western blot showed the expression level of p62, LC3 I and LC3 II in H446/cDDP cells under various medications treatment. **(G-H)** The cell viability was detected in LYPLAL1-DT-overexpressing H446 cells with VP-16 or PTX combined with HCQ or venetoclax treatment. **(I-K)** CCK-8 assay was used to detect the relative cell viability of H196/cDDP, H196/VP-16 and H196/PTX cells under various drug combinations (*, $P < 0.05$; **, $P < 0.01$; ***, $P < 0.001$)

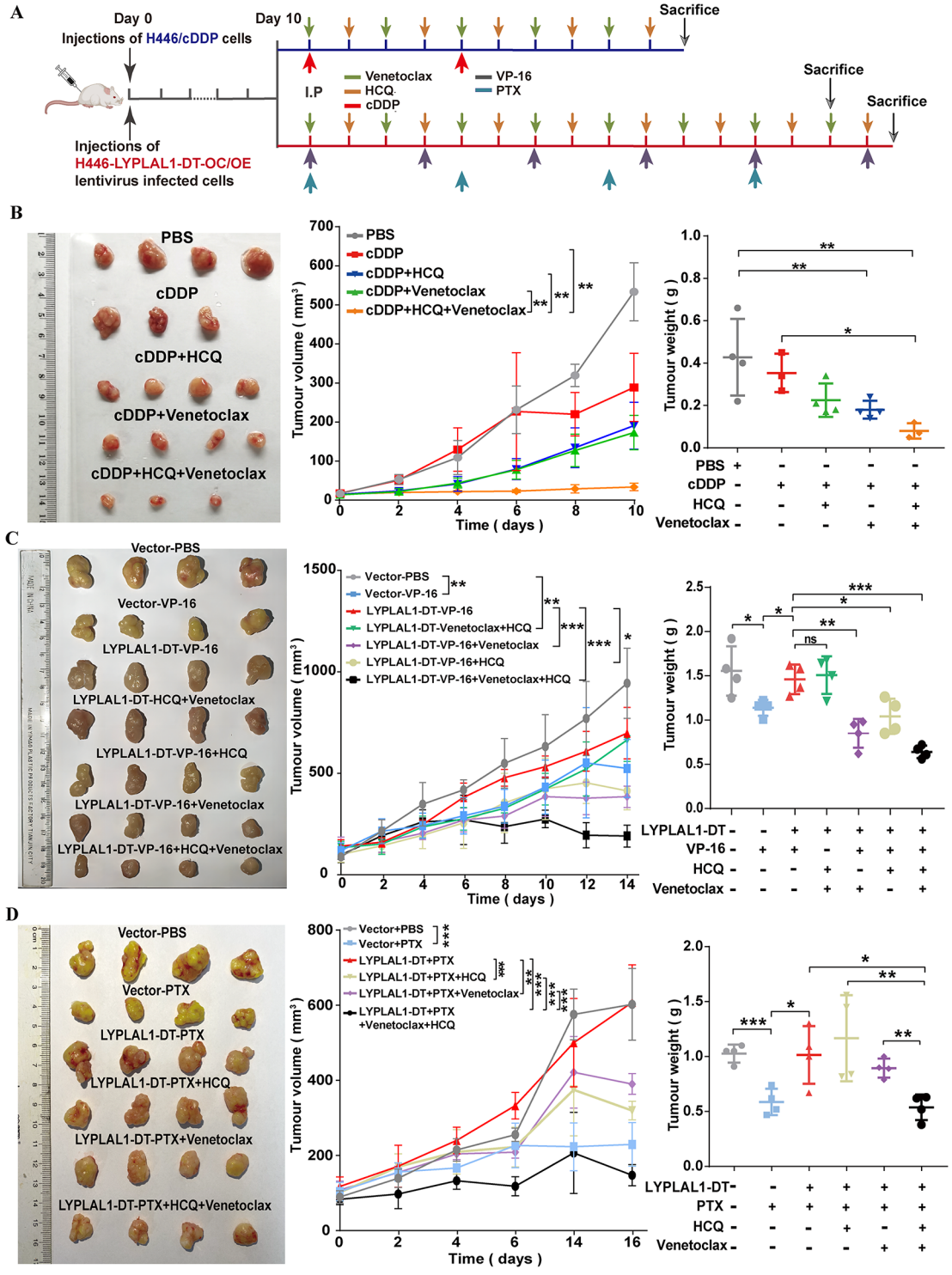

Fig. 7 Triple combination strategies remarkably induce cell death of chemoresistant SCLC in CDX mice model. **(A)** The schematic diagram of the in vivo experimental drug administration protocol. **(B-D)** Cell line-derived xenograft tumors were excised at the end of various drug treatments and the mean tumor volumes and weights were compared between groups (*, $P<0.05$; **, $P<0.01$; ***, $P<0.001$)

relapsed SCLC. Growing evidence showed that many malignant phenotypes may be driven by epigenetic factors, such as histone modification, chromatin remodeling and non-coding RNAs. For instance, high expression of EZH2, a histone methyltransferase gene, is a distinct feature of SCLC. The suppression of its target gene, SLFN11, was demonstrated by multiple chemoresistant SCLC models [34]. MYC, a key stemness-associated

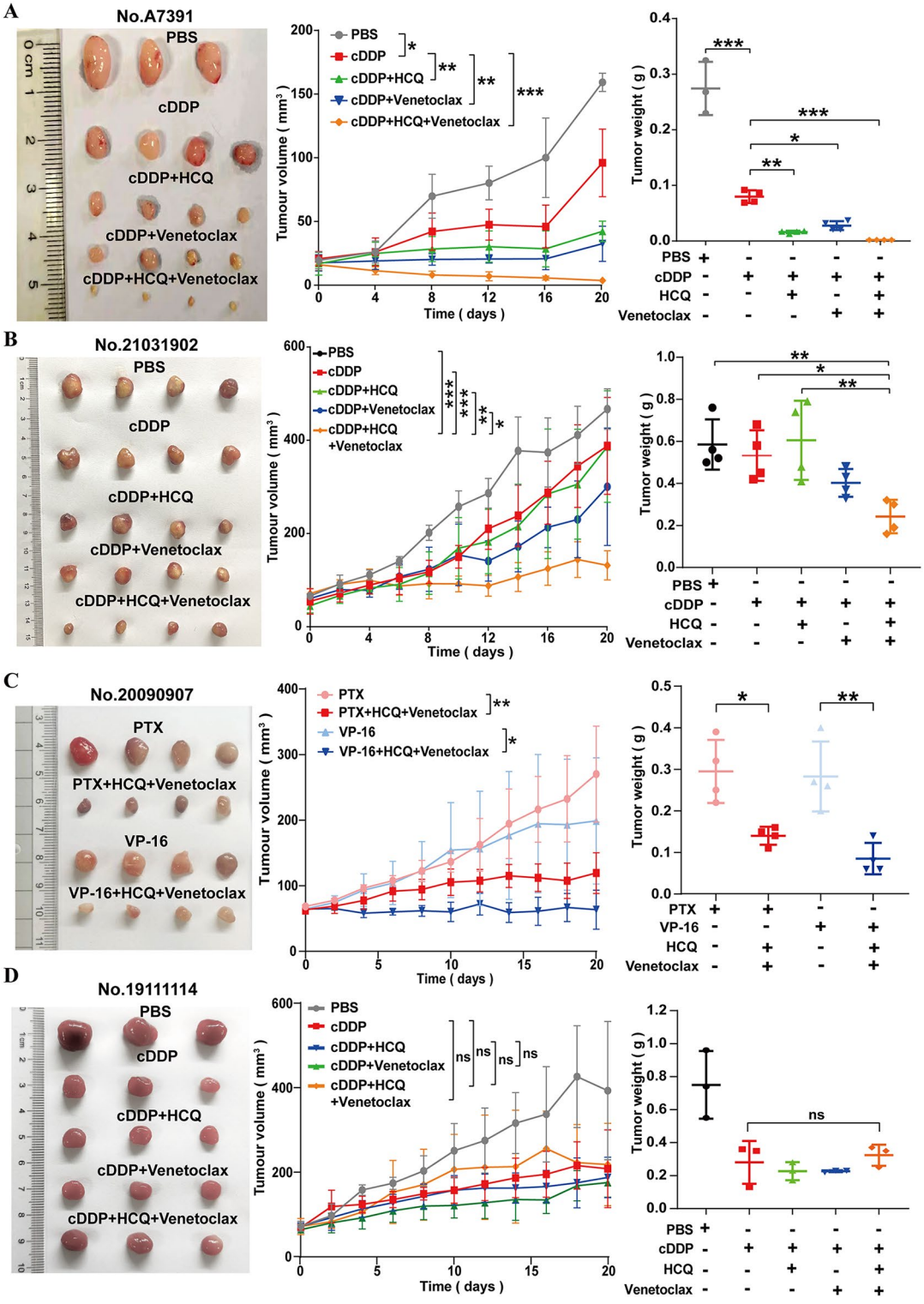

Fig. 8 Combinations of cDDP/VP-16/PTX, venetoclax and HCQ shrink the tumor volume of chemoresistant SCLC in PDX mice model. **(A-D)** Patient-derived xenograft tumors were excised at the end of various drug treatments and the mean tumor volumes and weights were compared between groups (*, $P < 0.05$; **, $P < 0.01$; ***, $P < 0.001$)

transcription factor, commonly amplified and drives proliferation, transdifferentiation of SCLC, is also associated with resistance to targeted therapies [35]. The treatment strategy targeting the EZH2/SLFN11 axis and MYC expression has yielded encouraging results [36, 37]. In the present study, we have identified that lncRNA LYPLAL1-DT is significantly upregulated in cDDP-, VP-16-, and PTX-resistant SCLC cells. It sequesters apoptosis through the LYPLAL1-DT/miR-204-5p/BCL2 axis and promotes autophagy by facilitating the assembly of the BECN1/PIK3C3 complex, thereby mediating multi-drug resistance of SCLC (Fig. 9). Furthermore, we have proposed a novel triple combination of venetoclax, HCQ, in conjunction with cDDP, VP-16 or PTX to combat refractory SCLC. Our experiments, conducted both in vitro and in vivo, have yielded promising results. Notably, our PDX model from four individuals has demonstrated that the triple combination is more effective in cases with high LYPLAL1-DT expression level compared to those with lower expression levels, all without any observed toxic effect. These findings define the prospect of our triple combination for future clinical applications.

More than three decades, cisplatin or plus etoposide is the standard first-line treatment. Despite initially high response rates to chemotherapy, most patients relapse within 6 months [5, 38]. Paclitaxel is commonly used in relapsed patients, with a response rate only about 20% [39], indicating the patient resistant for cisplatin or etoposide would not have benefit from paclitaxel due to MDR. Therefore, MDR has always been a major obstacle in improving the SCLC patients' survival. Several theories surrounding MDR have been proposed, of which apoptosis evasion and deregulation of autophagy are more intriguing ones [6, 20, 40]. Considering the characteristics of apoptosis inhibition and increased autophagy in refractory SCLC, we have developed a novel combination therapy approach to address this challenge. Venetoclax is a highly selective BCL2 inhibitor that has shown promise in hematologic malignancies [41]. Timothy L. Lochmann et al. demonstrated that venetoclax is effective in SCLC with high BCL2 expression [42]. However, venetoclax treatment did not exhibit high efficiency in some case since inhibition of BCL2 would activate autophagy, therefore induce new resistant mechanism [43]. Researchers have attempted to advance the antitumor effect of HCQ

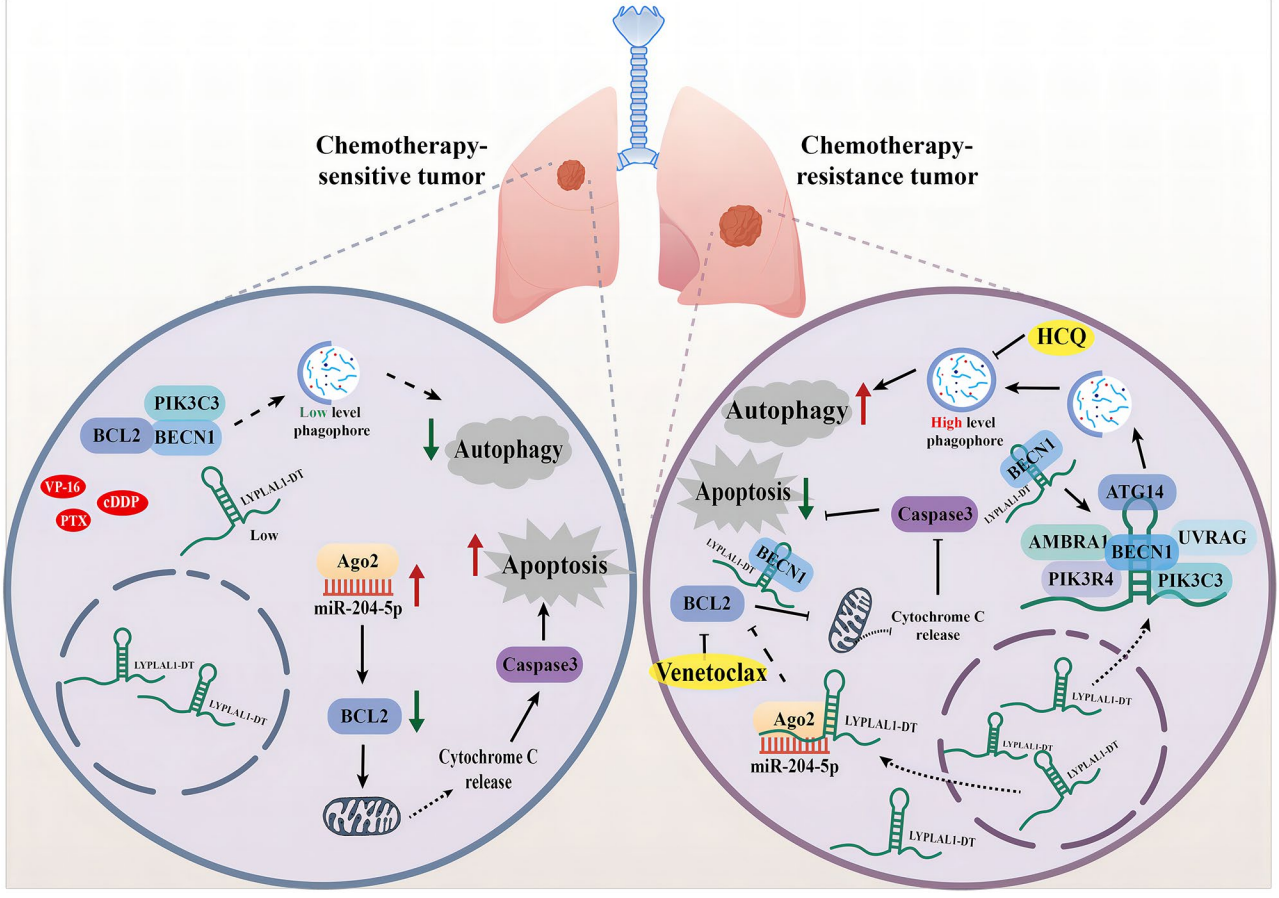

Fig. 9 The schematic diagram of LYPLAL1-DT involved in chemoresistance of SCLC

in clinical trials, either as a single agent or in combination with other agents [44, 45]. Here we create a novel protocol in which inhibiting BCL2 and autophagy simultaneously with venetoclax and HCQ, effectively shrank tumors in CDXs and PDX models with high LYPLAL1-DT expression, while showing little response in xenografts with low LYPLAL1-DT expression. This excellent protocol even caused the tumor cell to disappear in two PDX mice! We believe this strategy not only offers a novel treatment approach but also provides a basis for the development of LYPLAL1-DT as a promising biomarker for SCLC prognosis.

Current frontier has revealed that lncRNAs are implicated in various cancer progressing. However, only a few reported the profile, function and mechanism of lncRNA in SCLC [46–48]. More recently, Zhang C et al. made effort to construct the ceRNA networks in SCLC, further expanding the boundaries of lncRNAs [49]. LncRNA LYPLAL1-DT was screened and confirmed to have protective effects on endothelial cell in our previous work [31]. Furthermore, we identified the circulating levels of LYPLAL1-DT were significantly higher in SCLC compared to the normal control, indicating its potential roles in SCLC [32]. In the present study, we selected two SCLC cell lines, H446 and H196, as experimental cell models. According to the molecular subtypes of SCLC defined in 2019 and the report by Camille Tlemsani et al. in 2020, the H446 cell line is classified as N-type cells, whereas H196 is classified as Y-type cells [50, 51]. This distinction enables us to explore the role of LYPLAL1-DT across diverse cellular contexts and to assess the broader applicability of the triple-drug regimen. We illustrated the regulatory profile of LYPLAL1-DT under cDDP-, VP-16 and PTX treatment. We detected its upregulation in cDDP-, VP-16 and PTX-resistant SCLC cells and the positive correlation between its expression and dose or time under various drug treatment. We also unraveled that the high expression of LYPLAL1-DT is closely correlated to apoptosis inhibition and increased autophagy, with BCL2 and BECN1 identified as its downstream targets, which are the ideal target for clinical treatment. The results of PDX model further confirm that we identified LYPLAL1-DT as a chemoresistant biomarker in response to triple combination of ordinary chemicals, plus venetoclax and HCQ. Actually, a newest report demonstrated the role of LYPLAL1-DT in breast cancer [52]. An analysis of pan-cancer revealed that LYPLAL1-DT is related to the prognosis of thyroid cancer [53]. Based on GEO data, our pan-cancer analysis also showed positive relations of LYPLAL1-DT and various tumors (data not shown). These evidences indicate that LYPLAL1-DT may play a crucial role in cancers.

BCL2 and BECN1 are the key factors in regulating apoptosis and autophagy [54]. BCL2 is a well-established regulator that bridges apoptosis and autophagy. During the controlled scenario of autophagy, BCL2 is bound with the BH3-domain of BECN1, preventing the erroneous activation of autophagy according traditional theory [55]. Here we first revealed the molecular mechanism of LYPLAL1-DT as decoys to sponge the target miR-204-5p, further identifying BCL2 as a target gene for miR-204-5p to explain the down-regulating level of apoptosis in cDDP-, VP-16-, and PTX-resistant SCLC cells. However, high-expression of BCL2 contradicts the observation of abnormally high autophagy in SCLC cells following treatment of chemotherapy drugs. To explain the contradiction, we performed RIP experiments first, revealed an unexpected discovery of BECN1 and PIK3C3 in the immunoprecipitation complex associated with LYPLAL1-DT. The discovery was further validated through an RNA pull-down assay. Consequently, we propose that LYPLAL1-DT may induce the dissociation of BCL2 from BECN1, thereby contributing to the assembly of BECN1 and PIK3C3 complex, and consequently promoting autophagy in SCLC cells.

Some limitations still exist in our study. While we have demonstrated the involvement of LYPLAL1-DT in the assembly of BECN1/PIK3C3 complex through RIP and RNA pull-down assay, the exact binding sites still need to determine. If there are dynamic relations between the binding of BCL2 and BECN1, or LYPLAL1-DT and BECN1 are also needed to decode. Furthermore, the efficacy of the combined therapeutic approach has been confirmed by in vitro and in vivo experiments; however more clinical trials are required to assess its clinical efficiency in the future. Finally, if LYPLAL1-DT could be regarded as a biomarker for chemoresistance should be proven further in fresh SCLC tissues or serum samples of refractory patients.

Conclusion

In summary, we reported that upregulation of LYPLAL1-DT sequesters apoptosis through the LYPLAL1-DT/miR-204-5p/BCL2 axis and promotes autophagy by facilitating the assembly of the PtdIns3K complex, thereby meditating multi-drug resistance of SCLC. The triple combination of venetoclax, HCQ, in conjunction with cDDP, VP-16 or PTX overcomes refractory SCLC, especially in those with high LYPLAL1-DT expression. Our work deciphers a new molecular mechanism of chemoresistant SCLC, based on which offer a novel therapeutic approach for clinical trials, therefore provides a hopeful road for SCLC.

Abbreviations

BCL2	B-Cell Lymphoma 2
BECN1	Beclin-1
cDDP	Cisplatin
FISH	Fluorescence In Situ Hybridization
GAPDH	Glyceraldehyde 3-Phosphate Dehydrogenase
HCQ	Hydroxychloroquine
IF	Immunofluorescence
IHC	Immunohistochemical

IP	Immunoprecipitation
lncRNA	Long non-coding RNA
MDR	Multi-Drug Resistance
PDX	Patient-Derived Xenograft
PTX	Paclitaxel
RIP RNA	Immunoprecipitation
SCLC	Small Cell Lung Cancer
VP-16	Etoposide

Supplementary Information

The online version contains supplementary material available at https://doi.org/10.1186/s12943-024-02145-1.

Supplementary Material 1

Supplementary Material 2

Supplementary Material 3

Acknowledgements
Not applicable.

Author contributions
Shuxin Li, Jianyi Lv, Zhihui Li, Qiuyu Zhang and Jing Lu performed molecular biology and the animal experiments. Jianyi Lv, Xiaoyan Du and Shuxin Li wrote the main article. Zhenwen Chen and Xiaoyan Du designed the whole project and supervised all experiments. Changlong Li, Xueyun Huo, Meng Guo, and Xin Liu analyzed part of the data. Jinghui Wang, Shi Hanping and Deng Li provided support with experimental techniques and clinical samples. All authors read and approved the final article.

Funding
This work was supported by Beijing Municipal Public Welfare Development and Reform Pilot Project for Medical Research Institutes (JYY2023-14).

Data availability
No datasets were generated or analysed during the current study.

Declarations

Ethics approval and consent to participate
All animal experiments were performed in accordance with the relevant guidelines and regulations of Animal Experiments of Capital Medical University.

Consent for publication
Not applicable.

Competing interests
The authors declare no competing interests.

Author details
[1]School of Basic Medical Sciences, Capital Medical University, Beijing 100069, China
[2]Laboratory for Clinical Medicine, Capital Medical University, Beijing 100069, China
[3]Beijing Key Laboratory of Cancer Invasion and Metastasis Research, Beijing 100069, China
[4]Department of Medical Oncology, Beijing Chest Hospital, Beijing Tuberculosis and Thoracic Tumor Research Institute, Capital Medical University, Beijing 101149, China
[5]Department of Gastrointestinal Surgery/Clinical Nutrition, Capital Medical University Affiliated Beijing Shijitan Hospital, Beijing 100038, China

Received: 26 April 2024 / Accepted: 4 October 2024
Published online: 31 October 2024

References

1. Wang Q, Gumus ZH, Colarossi C, Memeo L, Wang X, Kong CY, et al. SCLC: Epidemiology, risk factors, genetic susceptibility, Molecular Pathology, Screening, and early detection. J Thorac Oncol. 2023;18(1):31–46.
2. Rudin CM, Brambilla E, Faivre-Finn C, Sage J. Small-cell lung cancer. Nat Rev Dis Primers. 2021;7(1):3.
3. Sonehara K, Tateishi K, Komatsu M, Yamamoto H, Hanaoka M. Lung immune prognostic index as a prognostic factor in patients with small cell lung cancer. Thorac Cancer. 2020;11(6):1578–86.
4. Khan P, Siddiqui JA, Maurya SK, Lakshmanan I, Jain M, Ganti AK, et al. Epigenetic landscape of small cell lung cancer: small image of a giant recalcitrant disease. Semin Cancer Biol. 2022;83:57–76.
5. Petty WJ, Paz-Ares L. Emerging strategies for the treatment of small cell lung Cancer: a review. JAMA Oncol. 2023;9(3):419–29.
6. Assaraf YG, Brozovic A, Goncalves AC, Jurkovicova D, Line A, Machuqueiro M, et al. The multi-factorial nature of clinical multidrug resistance in cancer. Drug Resist Updat. 2019;46:100645.
7. Mohammad RM, Muqbil I, Lowe L, Yedjou C, Hsu HY, Lin LT, et al. Broad targeting of resistance to apoptosis in cancer. Semin Cancer Biol. 2015;35(Suppl0):S78–103.
8. Klanova M, Klener P. BCL-2 proteins in Pathogenesis and Therapy of B-Cell Non-hodgkin Lymphomas. Cancers (Basel). 2020; 12(4).
9. Lee J, Sohn EJ, Yoon SW, Kim CG, Lee S, Kim JY, et al. Anti-metastatic effect of Dehydrocorydaline on H1299 Non-small Cell Lung Carcinoma cells via inhibition of Matrix metalloproteinases and B Cell Lymphoma 2. Phytother Res. 2017;31(3):441–8.
10. Delbridge AR, Grabow S, Strasser A, Vaux DL. Thirty years of BCL-2: translating cell death discoveries into novel cancer therapies. Nat Rev Cancer. 2016;16(2):99–109.
11. Zhang L, Lu Z, Zhao X. Targeting Bcl-2 for cancer therapy. Biochim Biophys Acta Rev Cancer. 2021;1876(1):188569.
12. Oltersdorf T, Elmore SW, Shoemaker AR, Armstrong RC, Augeri DJ, Belli BA, et al. An inhibitor of Bcl-2 family proteins induces regression of solid tumours. Nature. 2005;435(7042):677–81.
13. Jones JA, Mato AR, Wierda WG, Davids MS, Choi M, Cheson BD, et al. Venetoclax for chronic lymphocytic leukaemia progressing after ibrutinib: an interim analysis of a multicentre, open-label, phase 2 trial. Lancet Oncol. 2018;19(1):65–75.
14. DiNardo CD, Jonas BA, Pullarkat V, Thirman MJ, Garcia JS, Wei AH, et al. Azacitidine and Venetoclax in previously untreated Acute Myeloid Leukemia. N Engl J Med. 2020;383(7):617–29.
15. Lasica M, Anderson MA. Review of Venetoclax in CLL, AML and multiple myeloma. J Pers Med. 2021; 11(6).
16. Ong F, Kim K, Konopleva MY. Venetoclax resistance: mechanistic insights and future strategies. Cancer Drug Resist. 2022;5(2):380–400.
17. Bose P, Gandhi V, Konopleva M. Pathways and mechanisms of venetoclax resistance. Leuk Lymphoma. 2017;58(9):1–17.
18. Chong SJF, Zhu F, Dashevsky O, Mizuno R, Lai JX, Hackett L et al. Hyperphosphorylation of BCL-2 family proteins underlies functional resistance to venetoclax in lymphoid malignancies. J Clin Invest. 2023; 133(22).
19. Wu Q, Yang Z, Nie Y, Shi Y, Fan D. Multi-drug resistance in cancer chemotherapeutics: mechanisms and lab approaches. Cancer Lett. 2014;347(2):159–66.
20. Smith AG, Macleod KF. Autophagy, cancer stem cells and drug resistance. J Pathol. 2019;247(5):708–18.
21. Amaravadi RK, Lippincott-Schwartz J, Yin XM, Weiss WA, Takebe N, Timmer W, et al. Principles and current strategies for targeting autophagy for cancer treatment. Clin Cancer Res. 2011;17(4):654–66.
22. Levy JMM, Towers CG, Thorburn A. Targeting autophagy in cancer. Nat Rev Cancer. 2017;17(9):528–42.
23. Qadir MA, Kwok B, Dragowska WH, To KH, Le D, Bally MB, et al. Macroautophagy inhibition sensitizes tamoxifen-resistant breast cancer cells and enhances mitochondrial depolarization. Breast Cancer Res Treat. 2008;112(3):389–403.
24. Nguyen HG, Yang JC, Kung HJ, Shi XB, Tilki D, Lara PN Jr., et al. Targeting autophagy overcomes Enzalutamide resistance in castration-resistant prostate cancer cells and improves therapeutic response in a xenograft model. Oncogene. 2014;33(36):4521–30.
25. Gupta A, Roy S, Lazar AJ, Wang WL, McAuliffe JC, Reynoso D, et al. Autophagy inhibition and antimalarials promote cell death in gastrointestinal stromal tumor (GIST). Proc Natl Acad Sci U S A. 2010;107(32):14333–8.
26. Ma K, Li S, Huo X, Guo M, Du X, Li C, et al. Exploring the mechanism of cisplatin resistance by transcriptome sequencing and reversing the

chemoresistance by autophagy inhibition in small cell lung cancer. Biochem Biophys Res Commun. 2020;533(3):474–80.
27. Pandya G, Kirtonia A, Sethi G, Pandey AK, Garg M. The implication of long non-coding RNAs in the diagnosis, pathogenesis and drug resistance of pancreatic ductal adenocarcinoma and their possible therapeutic potential. Biochim Biophys Acta Rev Cancer. 2020;1874(2):188423.
28. Raziq K, Cai M, Dong K, Wang P, Afrifa J, Fu S. Competitive endogenous network of lncRNA, miRNA, and mRNA in the chemoresistance of gastrointestinal tract adenocarcinomas. Biomed Pharmacother. 2020;130:110570.
29. Li XL, Pongor L, Tang W, Das S, Muys BR, Jones MF et al. A small protein encoded by a putative lncRNA regulates apoptosis and tumorigenicity in human colorectal cancer cells. Elife. 2020; 9: e53734.
30. Adams BD, Parsons C, Walker L, Zhang WC, Slack FJ. Targeting noncoding RNAs in disease. J Clin Invest. 2017;127(3):761–71.
31. Zhu X, Liu Y, Cui J, Lv J, Li C, Lu J, et al. LncRNA LYPLAL1-DT screening from type 2 diabetes with macrovascular complication contributes protective effects on human umbilical vein endothelial cells via regulating the miR-204-5p/SIRT1 axis. Cell Death Discov. 2022;8(1):245.
32. Li S, Lv J, Zhang X, Zhang Q, Li Z, Lu J, et al. ELAVL4 promotes the tumorigenesis of small cell lung cancer by stabilizing LncRNA LYPLAL1-DT and enhancing profilin 2 activation. FASEB J. 2023;37(10):e23170.
33. Green DR, Llambi F. Cell death signaling. Cold Spring Harb Perspect Biol. 2015; 7(12).
34. Gardner EE, Lok BH, Schneeberger VE, Desmeules P, Miles LA, Arnold PK, et al. Chemosensitive Relapse in Small Cell Lung Cancer Proceeds through an EZH2-SLFN11 Axis. Cancer Cell. 2017;31(2):286–99.
35. Ireland AS, Micinski AM, Kastner DW, Guo B, Wait SJ, Spainhower KB, et al. MYC drives temporal evolution of small cell Lung Cancer subtypes by reprogramming neuroendocrine fate. Cancer Cell. 2020;38(1):60–78. e12.
36. Choudhury NJ, Lai WV, Makhnin A, Heller G, Eng J, Li B et al. A phase I/II study of valemetostat (DS-3201b), an EZH1/2 inhibitor, in combination with irinotecan in patients with recurrent small cell lung cancer. Clin Cancer Res. 2024; 30(17): 3697–3703.
37. Quintanal-Villalonga A, Kawasaki K, Redin E, Uddin F, Rakhade S, Durani V, et al. CDC7 inhibition impairs neuroendocrine transformation in lung and prostate tumors through MYC degradation. Signal Transduct Target Ther. 2024;9(1):189.
38. Wang S, Zimmermann S, Parikh K, Mansfield AS, Adjei AA. Current Diagnosis and Management of Small-Cell Lung Cancer. *Mayo Clin Proc*. 2019; 94(8): 1599–1622.
39. Yun T, Kim HT, Han JY, Yoon SJ, Kim HY, Nam BH, et al. A phase II study of Weekly Paclitaxel Plus Gemcitabine as a second-line therapy in patients with metastatic or recurrent small cell Lung Cancer. Cancer Res Treat. 2016;48(2):465–72.
40. Neophytou CM, Trougakos IP, Erin N, Papageorgis P. Apoptosis Deregulation and the Development of Cancer Multi-Drug Resistance. *Cancers (Basel)*. 2021; 13(17).
41. Guerra VA, DiNardo C, Konopleva M. Venetoclax-based therapies for acute myeloid leukemia. Best Pract Res Clin Haematol. 2019;32(2):145–53.
42. Lochmann TL, Floros KV, Naseri M, Powell KM, Cook W, March RJ, et al. Venetoclax is effective in small-cell lung cancers with high BCL-2 expression. Clin Cancer Res. 2018;24(2):360–9.
43. Valko Z, Megyesfalvi Z, Schwendenwein A, Lang C, Paku S, Barany N, et al. Dual targeting of BCL-2 and MCL-1 in the presence of BAX breaks venetoclax resistance in human small cell lung cancer. Br J Cancer. 2023;128(10):1850–61.
44. Ferreira PMP, Sousa RWR, Ferreira JRO, Militao GCG, Bezerra DP. Chloroquine and hydroxychloroquine in antitumor therapies based on autophagy-related mechanisms. Pharmacol Res. 2021;168:105582.
45. De Sanctis JB, Charris J, Blanco Z, Ramirez H, Martinez GP, Mijares MR. Molecular mechanisms of Chloroquine and Hydroxychloroquine used in Cancer Therapy. Anticancer Agents Med Chem. 2023;23(10):1122–44.
46. Zhang Y, Li Y, Han L, Zhang P, Sun S. SBF2-AS1: an oncogenic lncRNA in small-cell lung cancer. J Cell Biochem. 2019;120(9):15422–8.
47. Li J, Jing W, Jia W, Zhai X, Zhu H. Downregulation of lncRNA XR_429159.1 linked to Brain Metastasis in patients with Limited-Stage Small-Cell Lung Cancer. Front Oncol. 2021;11:603271.
48. Li D, Tong Q, Lian Y, Chen Z, Zhu Y, Huang W, et al. Inhibition of lncRNA KCNQ1OT1 improves apoptosis and Chemotherapy Drug Response in Small Cell Lung Cancer by TGF-beta1 mediated epithelial-to-mesenchymal transition. Cancer Res Treat. 2021;53(4):1042–56.
49. Zhang C, Zhou Y, Zhang B, Sheng Z, Sun N, Yuan B, et al. Identification of lncRNA, miRNA and mRNA expression profiles and ceRNA networks in small cell lung cancer. BMC Genomics. 2023;24(1):217.
50. Rudin CM, Poirier JT, Byers LA, Dive C, Dowlati A, George J, et al. Molecular subtypes of small cell lung cancer: a synthesis of human and mouse model data. Nat Rev Cancer. 2019;19(5):289–97.
51. Tlemsani C, Pongor L, Elloumi F, Girard L, Huffman KE, Roper N, et al. SCLC-CellMiner: a resource for small cell Lung Cancer Cell Line Genomics and Pharmacology based on genomic signatures. Cell Rep. 2020;33(3):108296.
52. Tang Y, Tian W, Zheng S, Zou Y, Xie J, Zhang J, et al. Dissection of FOXO1-Induced LYPLAL1-DT Impeding Triple-negative breast Cancer progression via mediating hnRNPK/beta-Catenin complex. Res (Wash D C). 2023;6:0289.
53. Su Y, Xu B, Li J, Shen Q, Lei Z, Ma M, et al. Identification of m6A-associated LncRNAs as predict factors for the immune infiltration and prognosis of thyroid cancer. Ann Med. 2023;55(1):1298–316.
54. Sorice M. Crosstalk of Autophagy and Apoptosis. *Cells*. 2022; 11(9).
55. Kang R, Zeh HJ, Lotze MT, Tang D. The beclin 1 network regulates autophagy and apoptosis. Cell Death Differ. 2011;18(4):571–80.

Publisher's note